Rotating Optical Microcavities with Broken Chiral Symmetry

Raktim Sarma,[1] Li Ge,[2,3] Jan Wiersig,[4] and Hui Cao[1,*]
[1]Department of Applied Physics, Yale University, New Haven, Connecticut 06520, USA
[2]Department of Engineering Science and Physics, College of Staten Island, CUNY, Staten Island, New York 10314, USA
[3]The Graduate Center, CUNY, New York, New York 10016, USA
[4]Institut für Theoretische Physik, Universität Magdeburg, Magdeburg, Postfach 4120, Germany
(Received 15 April 2014; published 5 February 2015)

We demonstrate in open microcavities with broken chiral symmetry that quasidegenerate pairs of copropagating-wave resonances are transformed by rotation to counterpropagating ones, leading to a striking change of emission directions. The rotation-induced relative change in output intensity increases exponentially with cavity size, in contrast to the linear scaling of the Sagnac effect. By tuning the degree of spatial chirality with cavity shape, we are able to maximize the emission sensitivity to rotation without spoiling the quality factor.

DOI: 10.1103/PhysRevLett.114.053903 PACS numbers: 42.55.Sa, 42.60.Da, 42.81.Pa

Light propagation in rotating systems has been studied as one of the most fundamental problems of electromagnetics [1–7]. So far, the majority of the studies have focused on conservative systems that are described by Hermitian Hamiltonians [8–10]. It is of fundamental interest to explore non-Hermitian systems in the rotating frame. For example, in an open cavity, both the resonance frequency and decay rate are modified by rotation [11,12]. Recent studies revealed an exponential dependence of the decay rate on the rotation speed, in contrast to the linear scaling of the frequency shift (Sagnac effect) [12]. Moreover, the rotation induces mode coupling in an open microcavity, resulting in crossing or anticrossing of decay rates and an abnormal Sagnac effect [13]. These studies illustrate that the open systems display much richer behaviors in the rotating frame than the closed ones.

In this Letter, we investigate the interplay between openness and chirality of rotating microcavities. Chirality has important implications in many areas of physics. Optical resonators may acquire structural chirality from shape deformation or boundary scattering, which induces asymmetric coupling between the clockwise (CW) and counterclockwise (CCW) propagating waves in the cavity [14–16]. With open boundary, the cavity resonances are dominated by either CW or CCW waves, thus possessing a preferred sense of rotation [17–22]. Such cavities with broken chiral symmetry are called chiral cavities.

However, it is not known what happens if a chiral cavity rotates, e.g., whether the Sagnac effect would survive in the absence of chiral symmetry, and how the intrinsic chirality is affected by rotation. In a nonrotating cavity with chiral symmetry, every resonance has balanced CW and CCW wave components, and the output intensity profile is symmetric. Rotation makes an individual mode dominated by either a CW or CCW wave, thus introducing asymmetry in the far-field pattern if CW and CCW waves have different output directions [23]. In a chiral cavity, even without rotation the breaking of chiral symmetry can make the far-field pattern asymmetric; it is not clear how rotation would further modify the emission profile.

To answer these questions, we investigate open microcavities with broken chiral symmetry in the rotating frame. Our calculations show that a quasidegenerate pair of copropagating-wave modes in the nonrotating chiral cavity evolve to counterpropagating ones at high rotation speed. The intrinsic chirality is thus removed by rotation, and the Sagnac effect is similar to that of a nonchiral cavity. However, the flip of propagation direction for one of the quasidegenerate modes will lead to a striking change of its far-field pattern, as long as the CW and CCW waves have distinct output directions. By tuning the cavity shape, we are able to vary the degree of chirality without spoiling the quality factor (see the Supplemental Material [24]). The maximal chirality results in the largest difference in CW and CCW outputs, making the emission profile most sensitive to rotation. The surprising enhancement of rotation sensitivity of chiral microcavities may open up the possibility of on-chip rotation sensors.

Let us first model a nonrotating chiral cavity. The asymmetric coupling between CW and CCW propagating waves can be described by an effective Hamiltonian [15,22]

$$H_0 = \begin{pmatrix} \omega_0 & 0 \\ 0 & \omega_0 \end{pmatrix} + \begin{pmatrix} \Gamma & V \\ \eta V^* & \Gamma \end{pmatrix}, \tag{1}$$

where ω_0 is the frequency of the unperturbed CCW and CW wave components. Their coupling leads to an overall frequency shift Γ and asymmetric transition elements V and ηV^*, where the deviation of $|\eta|$ from unity represents the degree of asymmetry. Diagonalization of H_0 gives the eigenfrequencies $\omega_\pm = \omega_0 + \Gamma \pm \sqrt{\eta}|V|$ (Supplemental Material [24]). The frequency splitting $\Delta\omega_0 = 2\sqrt{\eta}|V|$

results from the coupling of CW and CCW waves. The eigenvectors are composed of CW and CCW waves with relative intensity ratio $|\eta|$; thus, a higher asymmetry of the coupling leads to a stronger chirality of the eigenmodes.

When the cavity rotates, the Hamiltonian becomes (Supplemental Material [24])

$$H = H_0 + \begin{pmatrix} \Delta & 0 \\ 0 & -\Delta \end{pmatrix}, \tag{2}$$

where $\pm\Delta$ represents the frequency shift of CCW/CW wave by rotation. We assume the rotation speed is slow enough that $|\Delta|$ is linearly proportional to the rotation frequency Ω. For simplicity, we set $\Delta = \Omega$. The frequency splitting becomes $\Delta\omega = 2\sqrt{\eta|V|^2 + \Delta^2} = 2\sqrt{(\Delta\omega_0/2)^2 + \Omega^2}$ (Supplemental Material [24]). At low rotation speed, the additional frequency splitting induced by rotation (Ω) is much smaller than the original splitting ($\Delta\omega_0$), so the total splitting remains nearly constant $\Delta\omega \simeq \Delta\omega_0$. Only when Ω becomes comparable to $\Delta\omega_0$, the rotation-induced splitting becomes significant, and $\Delta\omega$ starts to grow with Ω. Eventually at $\Omega \gg \Delta\omega_0$, $\Delta\omega \approx 2\Omega$, the linear increase of $\Delta\omega$ with Ω recovers the Sagnac effect. Hence, the frequency splitting at $\Omega = 0$ causes a "dead zone" for the Sagnac effect [9]. In a chiral cavity, the dependence of $\Delta\omega$ on Ω is identical to that in a nonchiral cavity, as long as the value of $\eta|V^2|$ is kept the same [Fig. 1(a)]. Although without rotation both modes in the chiral cavity are dominated by CCW (CW) traveling waves for $|\eta| < 1$ ($|\eta| > 1$), one of them is transformed into a CW (CCW) traveling wave mode by rotation, and its frequency shifts in the opposite direction to the other mode, producing the same Sagnac effect as in the nonchiral cavity.

Next, we investigate how the emission patterns of chiral microcavities are modified by rotation. Without rotation, a pair of quasidegenerate modes is expected to have similar far-field patterns, because they are both dominated by either CW or CCW traveling waves. With rotation, one of them flips the propagation direction, and its far-field pattern will change dramatically if the CW and CCW waves have distinct output directions. To illustrate this, we simulate numerically open chiral cavities. We choose dielectric microdisks with the shape of asymmetric limaçon, which have a high-quality (Q) factor and small frequency splitting $\Delta\omega_0$ [22]. The microdisk can be regarded as a two-dimensional cavity, as the disk thickness is much smaller than the radius. In the polar coordinates, the cavity boundary is described by $r(\theta) = R[1 + \epsilon_1\cos(\theta) + \epsilon_2\cos(2\theta + \delta)]$, where R is the radius, ϵ_1 and ϵ_2 are the deformation parameters, and δ determines the degree of chirality (to be discussed later). We calculate the resonant modes in the nonrotating cavity using the finite-difference frequency-domain method [25]. As an example, we investigate a pair of quasidegenerate modes with the normalized frequency $kR \simeq 6.2$ in a cavity of $\delta = 1.94$ ($k = 2\pi/\lambda$, and

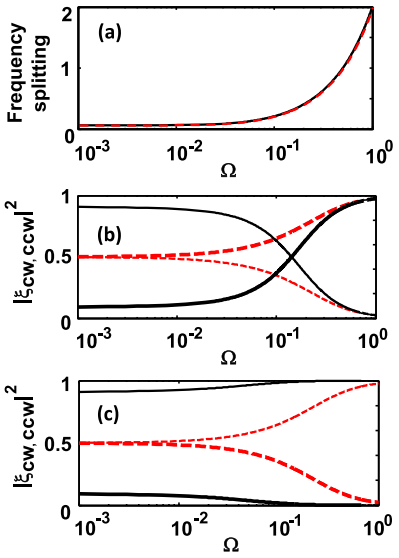

FIG. 1 (color online). Comparison of Sagnac effect in a rotating microcavity with chiral symmetry ($\eta = 1$, dashed line) and without chiral symmetry ($\eta = 0.1$, solid line). The value of $\eta|V|^2$ is kept the same. (a) (Dimensionless) frequency splitting for a pair of quasidegenerate modes as a function of rotation frequency Ω. [(b) and (c)] Evolution of CW (thick line) and CCW (thin line) traveling-wave components in the quasidegenerate modes with rotation. In the symmetric cavity ($\eta = 1$), at low rotation speed the eigenmodes remain standing-wave modes with equal weights of CCW and CW components, and their frequency difference is barely changed by rotation. When the rotation speed is sufficiently high, one mode evolves to a CCW traveling-wave mode and the other one to a CW traveling-wave mode, and their frequency difference starts to grow significantly with Ω. In a chiral cavity ($\eta = 0.1$), the evolution of frequency splitting with rotation is identical to that of the symmetric cavity. Without rotation, both modes are dominated by CCW traveling waves, but one of them (b) transforms into a CW traveling wave mode at high Ω.

λ is the wavelength in vacuum). Both modes contain more CW wave components than the CCW ones (Supplemental Material [24]). Their spatial chirality is characterized by the difference between CW and CCW wave intensities normalized by the (dominant) CW wave intensity, and its value is equal to 0.25. Both modes generate directional emissions, as shown in Fig. 2(a). By separating the CW and CCW wave components outside the cavity, we find that the main output direction of the CW wave is $\theta \simeq 0.7$ and $\theta \simeq 2.8$ for the CCW wave [Fig. 2(b)]. Because of the dominant presence of the CW wave in the quasidegenerate pair, their far-field patterns are similar to that of the CW wave.

Next, we consider the asymmetric limaçon cavity rotating with a constant angular velocity Ω around a fixed axis perpendicular to the cavity plane. In the rotating frame where the cavity is stationary, the Maxwell equations remain the same but the constitutive relations are modified [26,27]. Various methods have been developed to study

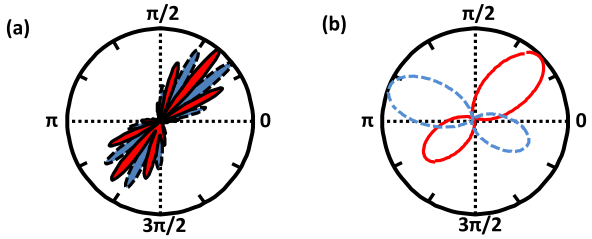

FIG. 2 (color online). Far-field emission intensity patterns of a pair of quasidegenerate modes ($\lambda = 598$ nm) in a nonrotating dielectric disk ($n = 3.0$) of asymmetric limaçon shape ($R = 591$ nm, $\epsilon_1 = 0.1$, $\epsilon_2 = 0.075$, $\delta = 1.94$). (a) Angular distributions of emission intensities at a distance of $r = 50R$ from the cavity center for both modes, which have similar output directions. (b) Far-field patterns of CW (red solid line) and CCW (blue dashed line) wave components in the resonances, exhibiting distinct output directions.

photonic structures in the rotating frame [4,27–32]. Here we used a finite-difference time-domain algorithm, adapted to the rotating frame [12], to calculate the mode profile and emission pattern. As shown in Fig. 3, one of the two modes in Fig. 2 switches from CW to CCW traveling wave, while the other one remains CW. Consequently, their output directions become very different.

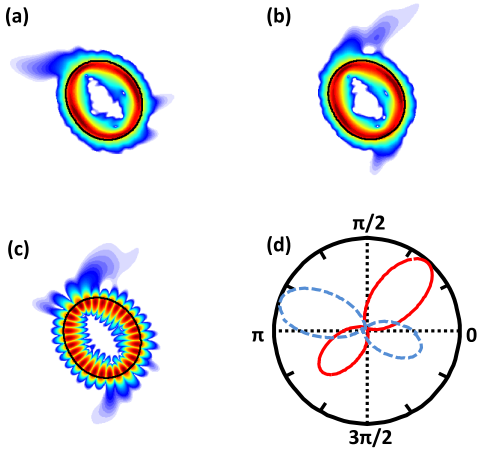

FIG. 3 (color online). Emission from the rotating asymmetric limaçon cavity with the same parameters as the stationary one in Fig. 2. [(a), (b)] Spatial distributions of field intensities for a pair of degenerate modes, which correspond to the stationary modes in Fig. 2, at the normalized rotation frequency $\Omega R/c = 10^{-3}$. The intensities outside the cavity are enhanced to illustrate that the main output directions of the two modes are different, even though they have the same output directions without rotation [Fig. 2(a)]. (c) Spatial distribution of field intensity for one of the quasidegenerate modes in the nonrotating cavity. It is dominated by CW wave. When the cavity rotates in the CCW direction, this mode switches from CW to CCW wave, and the main output direction is changed dramatically. (d) Angular distribution of far-field intensity for the pair of modes shown in (a) and (b) in the rotating cavity.

The striking change of output direction by rotation originates from the breaking of chiral symmetry in the open microcavity. Even when the cavity is at rest, the resonances already acquire a preferred sense of rotation, as the quasidegenerate pairs are both dominated by CW or CCW traveling waves (Fig. 2 and Supplemental Material Fig. S1 [24]). However, as the microcavity starts rotating, the intrinsic chirality of the resonances is removed, and every pair has one mode CW dominated and the other CCW dominated.

The direction of rotation determines which one of the quasidegenerate pair, the higher or lower frequency mode, will flip the propagation direction and exhibit a dramatic change in the output direction. For example, the two modes in Fig. 2 are both dominated by CW traveling waves at rest; if the rotation is in the CCW (CW) direction, the lower (higher) frequency mode will transform to CCW, and its frequency will decrease (increase) further with rotation. Hence, by measuring the emission frequency in the main output direction of the CCW or CW wave, we can identify the direction of rotation.

In reality, both of the quasidegenerate modes are often excited simultaneously, and their relative phases depend on the excitation condition, which varies from one experimental setting to another. The interference of their output fields determines the emission pattern, which will be modified by rotation. To calculate quantitatively the change of emission pattern by rotation, we simulate a generic case (Supplemental Material [24]). Seed pulses are launched from 10 randomly chosen locations inside the cavity to excite the quasidegenerate modes. The photodetectors are assumed to be stationary in the rotating frame and placed at a distance of $3R$ from the cavity center. After the seed pulses pass by, the photodetectors are turned on to measure the emission intensity. Figure 4(a) plots the temporally integrated intensity I_e as a function of the emission angle θ for the quasidegenerate pair of modes in Fig. 2. The irregular oscillations of I_e with θ result from the beating of the two excited modes, which depend on their initial phase difference.

The excitation condition is kept the same when the rotation speed Ω increases. With increasing Ω, some peaks of $I_e(\theta)$ increase while others decrease [Fig. 4(a)], as the copropagating wave resonances evolve to counterpropagating ones. The main emission peak at $\theta \simeq 0.7$ is from the CW wave, and its intensity decreases as one of the modes is converted to CCW wave by rotation. Meanwhile, the secondary peaks at $\theta \simeq 2.8$ increase with Ω, since they are from the CCW wave. In Fig. 4(b), the relative changes in the main peak intensity and its ratio to the secondary peak intensity are plotted vs the normalized rotation speed $\Omega R/c$ (c is the speed of light in vacuum). The latter is about 2 times greater than the former.

To compare with the Sagnac effect, we calculate the frequency splitting $\Delta\omega$ of these two modes in a circular

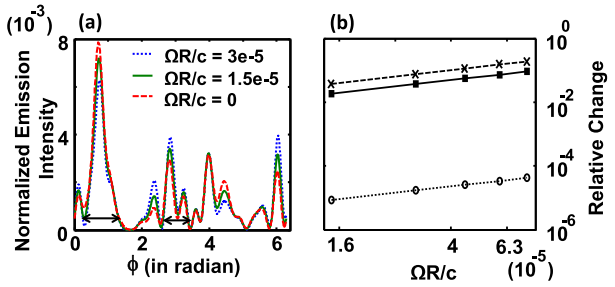

FIG. 4 (color online). Rotation-induced change in emission pattern of the same cavity as the one in Fig. 3, when both quasidegenerate modes are excited simultaneously. (a) Angular distribution of the emission intensity I_e at a distance of $r = 3R$ from the cavity center at three rotation speeds. To show the change in the emission profile, $I_e(\theta)$ is normalized ($\int_0^{2\pi} I_e(\theta)d\theta = 1$). (b) Relative changes in the main emission peak intensity (at $\theta = 0.73$) (solid squares and solid line) and in the ratio of main peak intensity over the secondary peak intensity (at $\theta = 2.79$) (crosses and dashed line) vs the normalized rotation frequency $\Omega R/c$. Both peak intensities are integrated over a range of emission angles marked by the double-arrowed segments in (a). For comparison, relative changes of resonant frequencies $\Delta\omega/\omega_0$ are plotted for circular cavities with the same area and refractive index (open circles and dotted line). The symbols represent the numerical data, and the straight lines are linear fit of the data in the log-log plot, which gives the slope. The values of the slope are (from top to bottom) 2.4×10^3, 1.2×10^3, and 5.7×10^{-1}, respectively. The rotation-induced changes of output intensity are much larger than that of the resonance frequency.

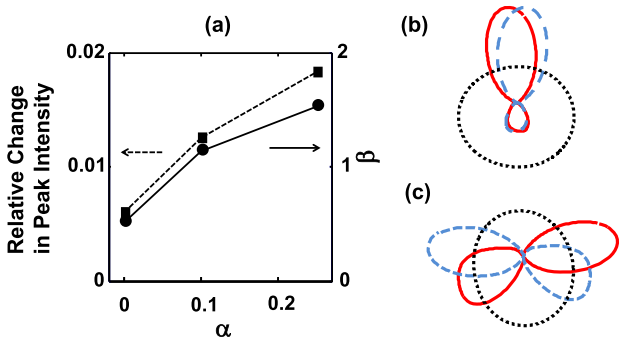

FIG. 5 (color online). Output sensitivity to rotation for the asymmetric limaçon cavity with varying degree of spatial chirality. The cavity parameters are the same as those in Fig. 2 except for the value of δ. (a) Relative change of the emission intensity in the main output direction (solid squares and dashed line) as a function of spatial chirality α for the quasidegenerate modes in Fig. 2. The rotation frequency is fixed at $\Omega R/c \simeq 1.5 \times 10^{-5}$. The difference between the emission patterns for CW and CCW waves in the nonrotating cavity is quantified by β (solid circles and solid line), which is also plotted against α. With increasing spatial chirality α, CW and CCW outputs become more distinct, enhancing the emission sensitivity to rotation. [(b), (c)] Far-field patterns for CW wave (red solid line) and CCW wave (blue dashed line) in two cavities with $\delta = 0$ (b) and 2.75 (c). The dotted line marks the cavity boundary. At $\delta = 0$, both CW and CCW waves emit predominantly in the direction close to $\theta = \pi/2$ (b), and the slight difference of their emission directions is a result of wave effects in the wavelength-scale cavity [33]. As δ increases from 0 to π, the main emission direction of the CW wave moves towards $\theta = 0$ and the CCW wave towards $\theta = \pi$; meanwhile, the secondary emission peak, which is in the opposite direction of the main peak, grows monotonically.

cavity with the same area and refractive index as the asymmetric limaçon. The normalized frequency splitting $\Delta\omega/\omega_0$, where ω_0 is the resonant frequency in the nonrotating cavity, gives the relative change of the resonant frequency by rotation. A linear fit of the data in the log-log plot of Fig. 4(b) finds the slopes, which reflect the sensitivity to rotation. The slope for the relative change in the main emission peak intensity of the asymmetric limaçon cavity is about 3 orders of magnitude greater than the slope of the relative frequency shift in the circular cavity.

To enhance the emission sensitivity to rotation, we tune the degree of spatial chirality by varying δ of the limaçon cavity. For $\delta = m\pi$ (m is an integer), the cavity has the chiral symmetry [$r(-\theta) = r(\theta)$]; as δ deviates from $m\pi$, the chiral symmetry is broken. We compute the spatial chirality α of the quasidegenerate modes, shown in Fig. 2, in the nonrotating cavity with varying δ (Supplemental Material [24]). As δ increases from 0 to π, α first grows and reaches the maximum at $\delta \simeq 1.94$, then drops to zero at $\delta = \pi$ [22]. We simulate the rotating cavities with different δ and find that the relative change of the main emission peak intensity increases monotonically with α at a fixed rotation speed [Fig. 5(a)].

To interpret this result, we compare the far-field patterns for CW and CCW waves in the nonrotating cavities with different δ values. The difference between CW and CCW emission patterns is quantified by $\beta = \int_0^{2\pi} |I_{\mathrm{CW}}(\theta) - I_{\mathrm{CCW}}(\theta)|d\theta$, which is plotted as a function of α in Fig. 5(a). Both $I_{\mathrm{CW}}(\theta)$ and $I_{\mathrm{CCW}}(\theta)$ are normalized ($\int_0^{2\pi} I_{\mathrm{CW,CCW}}(\theta)d\theta = 1$). The monotonic increase of β with α indicates that the emission patterns for CW and CCW waves become more distinct at higher chirality; consequently, the mode emission pattern changes more significantly by rotation. The maximal spatial chirality provides the highest sensitivity of microcavity output to rotation.

Because of our limited computing power, the simulated microcavities have the size R comparable to the vacuum wavelength λ. With an increase of R, the emission sensitivity to rotation is expected to increase, because the spatial chirality increases with cavity size [22], along with an increase of the Q factor and a decrease of the intrinsic frequency splitting $\Delta\omega_0$. The minimum rotation speed Ω_c to produce a measurable change of the emission profile is proportional to the size of the dead zone $\Delta\omega_0$ (Supplemental Material [24]). As observed in previous studies [34,35], our numerical simulation of nonrotating cavities reveals that $\Delta\omega_0$ reduces exponentially as kR

increases. This leads to an exponential decrease of Ω_c with R (Supplemental Material [24]). Thus, we can estimate Ω_c as a function of R from the numerical data of very small cavities (Supplemental Material [24]). For an asymmetric limaçon cavity with $R = 25$ μm, a rotation speed as low as 1 rpm can cause a noticeable ($\sim$1%) change in the main emission peak intensity.

We are grateful to Professor Michel Digonnet for stimulating discussion and useful information about rotation sensing. This work is funded partly by NSF under Grants No. ECCS-1128542 and No. DMR-1205307 and by DFG under Grant No. WI1986/6-1.

*hui.cao@yale.edu

[1] E. J. Post, Rev. Mod. Phys. **39**, 475 (1967).
[2] W. W. Chow, J. Gea-Banacloche, L. M. Pedrotti, V. E. Sanders, W. Schleich, and M. O. Scully, Rev. Mod. Phys. **57**, 61 (1985).
[3] M. Skorobogatiy and J. D. Joannopoulos, Phys. Rev. B **61**, 15554 (2000).
[4] B. Z. Steinberg, Phys. Rev. E **71**, 056621 (2005).
[5] M. Terrel, M. Digonnet, and S. Fan, Laser Photonics Rev. **3**, 452 (2009).
[6] C. Ciminelli, F. DellOlio, C. E. Campanella, and M. N. Armenise, Adv. Opt. Photonics **2**, 370 (2010).
[7] C. Sorrentino, J. R. E. Toland, and C. P. Search, Opt. Express **20**, 354 (2012).
[8] S. Sunada and T. Harayama, Phys. Rev. A **74**, 021801 (2006).
[9] S. Sunada and T. Harayama, Opt. Express **15**, 16245 (2007).
[10] T. Harayama, S. Sunada, and T. Miyasaka, Phys. Rev. E **76**, 016212 (2007).
[11] J. Scheuer, Opt. Express **15**, 15053 (2007).
[12] R. Sarma, H. Noh, and H. Cao, J. Opt. Soc. Am. B **29**, 1648 (2012).
[13] L. Ge, R. Sarma, and H. Cao, Phys. Rev. A **90**, 013809 (2014).
[14] J. Wiersig, Phys. Rev. A **84**, 063828 (2011).
[15] J. Wiersig, Phys. Rev. A **89**, 012119 (2014).
[16] J. Yang, X. Xiao, C. Hu, W. Zhang, S. Zhou, and J. Zhang, Nano Lett. **14**, 704 (2014).
[17] G. D. Chern, H. E. Tureci, A. D. Stone, R. K. Chang, M. Kneissl, and N. M. Johnson, Appl. Phys. Lett. **83**, 1710 (2003).
[18] J. Wiersig, S. W. Kim, and M. Hentschel, Phys. Rev. A **78**, 053809 (2008).
[19] J. Wiersig, Opt. Express **16**, 5874 (2008).
[20] M. Hentschel and T. Y. Kwon, Opt. Lett. **34**, 163 (2009).
[21] M. Hentschel, T. Kwon, M. A. Belkin, R. Audet, and F. Capasso, Opt. Express **17**, 10335 (2009).
[22] J. Wiersig, A. Eberspächer, J. B. Shim, J. W. Ryu, S. Shinohara, M. Hentschel, and H. Schomerus, Phys. Rev. A **84**, 023845 (2011).
[23] L. Ge, R. Sarma, and H. Cao, arXiv:1404.5289.
[24] See Supplemental Material at http://link.aps.org/supplemental/10.1103/PhysRevLett.114.053903 for calculation details.
[25] COMSOL Multiphysics, version 3.5.
[26] T. Shiozawa, Proc. IEEE **61**, 1694 (1973).
[27] B. Z. Steinberg, A. Shamir, and A. Boag, Phys. Rev. E **74**, 016608 (2006).
[28] J. Scheuer and A. Yariv, Phys. Rev. Lett. **96**, 053901 (2006).
[29] B. Z. Steinberg and A. Boag, J. Opt. Soc. Am. B **24**, 142 (2007).
[30] C. Peng, R. Hui, X. Luo, Z. Li, and A. Xu, Opt. Express **16**, 5227 (2008).
[31] D. Hah and D. Zhang, Opt. Express **18**, 18200 (2010).
[32] R. Novitski, J. Scheuer, and B. Z. Steinberg, Phys. Rev. E **87**, 023303 (2013).
[33] B. Redding, L. Ge, Q. Song, J. Wiersig, G. S. Solomon, and H. Cao, Phys. Rev. Lett. **108**, 253902 (2012).
[34] E. Doron and S. D. Frischat, Phys. Rev. Lett. **75**, 3661 (1995).
[35] G. Hackenbroich, E. Narimanov, and A. D. Stone, Phys. Rev. E **57**, R5 (1998).